ChemComm

COMMUNICATION

View Article Online
View Journal | View Issue

Cite this: *Chem. Commun.*, 2023, **59**, 14689

Received 15th September 2023,
Accepted 16th November 2023

DOI: 10.1039/d3cc04573k

rsc.li/chemcomm

Reversing the ion transport selectivity through arm modification of an artificial molecular hourglass†

Wen-Long Huang,[a] Xu-Dong Wang,[a] Yu-Fei Ao,[ab] Qi-Qiang Wang[ab] and De-Xian Wang *[ab]

An arm modification strategy, by replacing relatively rigid, electron-deficient side arms with flexible ether chain arms and linking them onto a tetraoxacalix[2]arene[2]triazine skeleton, was utilized to design an artificial molecular hourglass. The planar bilayer experiments confirmed the unimolecular channel mechanism and suggested reversed ion selectivity from the previously reported anion selectivity to weak cation selectivity.

Ion homeostasis—the intracellular and extracellular ion concentration balance state, is of vital importance for normal physiological functions of cells and organisms.[1] Ion channels and ion transporters play key roles in the regulation of ion homeostasis and cellular functions. Chloride channels, for example, are responsible for stabilizing the resting membrane potential, regulating electrical excitability, producing transepithelial fluid and maintaining cellular volume.[1,2] Malfunction or defectiveness of chloride channels could lead to serious ion channelopathies such as cystic fibrosis (CF),[3] Batter's syndrome and Dent's disease.[2,4] ClC Cl^- channels represent the main family of chloride channels and possess characteristics of high Cl^-/K^+ selectivity and coupling behaviour between ion conduction and gating.[5] The unique functions of ClC Cl^- channels are determined by the hourglass-shape pore and selectivity filter. The filter locates at the narrowest centre of the pore and provides partially charged binding sites to stabilize and permit rapid diffusion of chloride. The mysterious structure and function of ClC Cl^- channels inspired chemists to design simple molecular models to explore the structure–function relationship and to probe the structural principle of the channel protein, as well to explore the potential applications of artificial channel molecules in biomedicine, drug delivery and sensors, and for diagnosis and therapy.[6,7]

Two structural principles, *i.e.*, macrocyclic skeleton (self-assembled or single macrocycle) and non-covalent driving forces (binding sites), are usually the key concerns for designing synthetic chloride channel molecules. Despite the importance in fundamental science and biology, it is extremely difficult to construct artificial channels that show high Cl^-/K^+ selectivity as the natural channel protein does because of the large size and high hydration energy of chloride in comparison with potassium.[8] In previous work, we have designed the molecular hourglass **1** using (1) tetraoxacalix[2]arene[2]triazine as the central and narrow part, (2) electron-deficient aromatic imides tethered by glycol chains on both sides of the macrocycle as the extending arms, and (3) phenylalanine moieties as the terminal heads (Fig. 1a).[9a] The advantages of the functional central macrocycle and anion–π driving force endowed moderate Cl^-/K^+ selectivity (P_{Cl^-}/P_{K^+} = 1.90). Furthermore, a "mutation" strategy through replacing the inert benzene rings with active phenol rings enabled a cooperative anion–π and hydrogen bonding interaction mode at the central macrocycle.[9b] Such structural change provided a second molecular hourglass with high Cl^- selectivity (P_{Cl^-}/P_{K^+} up to 12.31). Besides, owing to the sensitivity of terminal phenylalanine moieties to the environment, the second molecular hourglass showed pH-dependent transport behaviours. As a key constructive component of the molecular hourglass, we wondered how the electron-deficient arms would affect the chloride transport selectivity. To probe the contribution of the hourglass arms, we herein designed a new molecular hourglass **2** through an arm modification strategy on the initial molecular hourglass **1** (Fig. 1b). Specifically, electron-rich 1,3-dialkoxybenzene moieties are applied instead of electron-deficient aromatic imides as the main component of the arms. The synthesis, ion transport activity, and ion selectivity of molecular hourglass **2** are presented.

The artificial molecular hourglass **2** was synthesized smoothly through monomer preparation, one-pot macrocyclization, and

[a] *Beijing National Laboratory for Molecular Sciences, CAS Key Laboratory of Molecular Recognition and Function, Institute of Chemistry, Chinese Academy of Sciences, Beijing 100190, China. E-mail: dxwang@iccas.ac.cn*
[b] *University of Chinese Academy of Sciences, Beijing 100049, China*

† Electronic supplementary information (ESI) available. See DOI: https://doi.org/10.1039/d3cc04573k

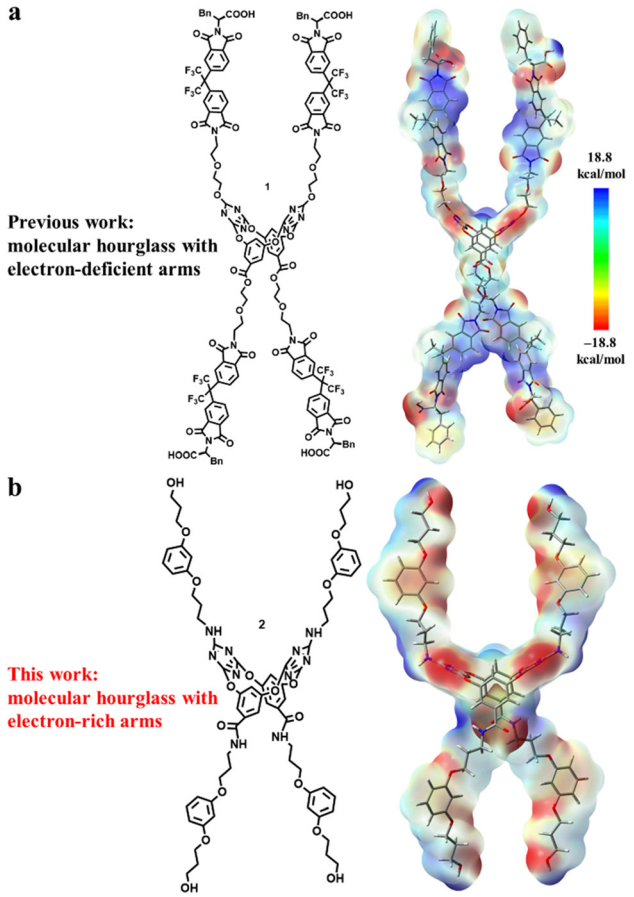

Fig. 1 The structures and electrostatic potentials of artificial molecular hourglass **1** (a) and **2** (b). Blue and red bars represent electron-deficient and electron-rich regions, respectively.

subsequent derivatizations (Scheme 1, also see ESI,† Section S2). Starting with commercially available raw materials of resorcinol and two alkyl bromides, primary amine fragment **5** was firstly prepared with modest yield. The pivotal resorcinol monomer **6** was obtained by condensation reaction between **5** and 3,5-dihydroxybenzoic acid. One-pot macrocyclization between resorcinol monomer **6** and cyanuric chloride produced tetraoxacalix[2]arene[2]triazine macrocycle **7** in 30% yield. Nucleophilic substitution reaction between **7** and primary amine fragment **5** provided the precursor compound **8** in 79% yield. The benzyl groups of **8** were removed under H_2 gas with Pd/C to afford the target molecular hourglass **2** in 32% yield.

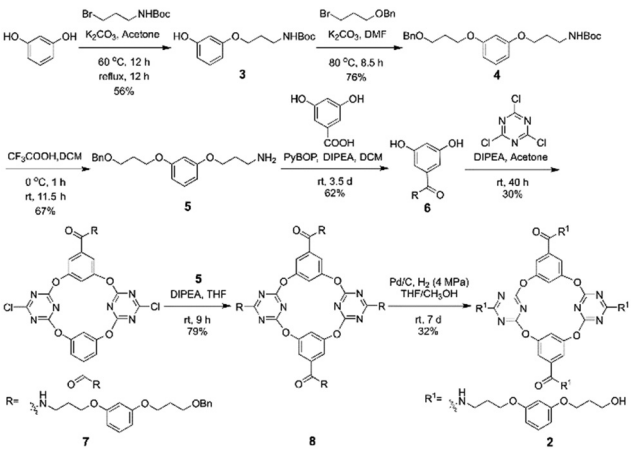

Scheme 1 The synthesis of artificial molecular hourglass **2**.

The anion and cation association ability of artificial molecular hourglass **2** was initially assessed through ^{1}H NMR titration experiments. Upon the gradual addition of $Bu_4N^+Cl^-$ to the solution of **2** in d_6-acetone, proton H14 within the macrocycle cavity shifted upfield, and then downfield, and protons H12 and H13 moved downfield continuously (Fig. 2c and Fig. S1, ESI†), which suggested anion–π binding between Cl^- and the triazine rings.[9a,10] The continuous downfield motion of amide proton H11 and amino proton H11' indicated hydrogen bonding interactions between Cl^- and these two kinds of protons. The peak shape variation of protons H5 and H5′, and partial downfield movement of aryl protons (H4, H6, H7, *etc.*) and alkyl protons (H1, H10, *etc.*) manifested the non-covalent interactions between arm components with Cl^-. Compared with Cl^-, with the continuous addition of $K^+PF_6^-$, these protons showed relatively smaller chemical shift changes ($\Delta\delta$ < 0.08 ppm, Fig. 2b and Fig. S2, ESI†). However, these changes still disclosed non-covalent contact of K^+ to the components of the molecular hourglass. The titration experiments indicated that **2** possessed the ability to bind Cl^- and K^+, but showed stronger affinity toward Cl^- (association constant: K_1 = 1067.0 ± 28.8 M^{-1}, K_2 = 23.1 ± 0.2 M^{-1}, with a 1 : 2 host–guest stoichiometry) than K^+ (K_1 = 242.9 ± 35.2 M^{-1}, K_2 = 4.2 ± 0.1 M^{-1}) (Table S1, ESI†).

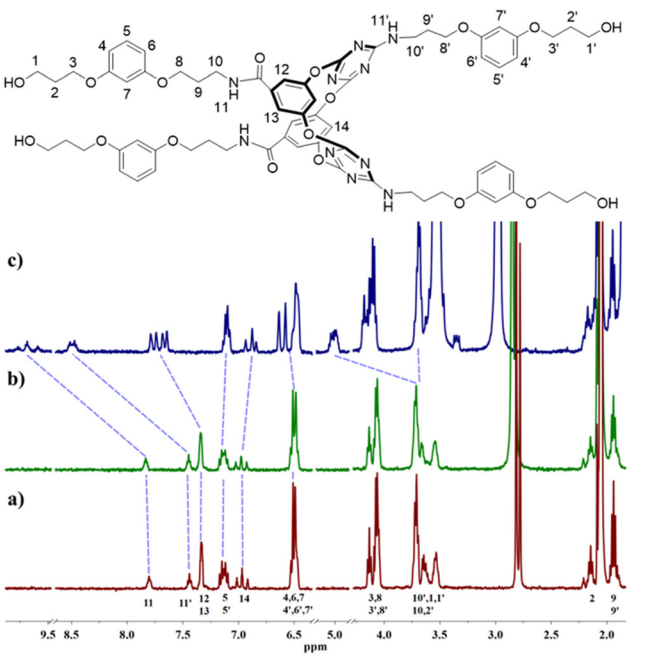

Fig. 2 (a) Proton chemical shift of **2** (1 × 10^{-3} mol L^{-1}) and chemical shift changes upon addition of (b) $K^+PF_6^-$ (46.4 × 10^{-3} mol L^{-1}) or (c) $Bu_4N^+Cl^-$ (45.4 × 10^{-3} mol L^{-1}) in d_6-acetone at room temperature. For clarity, partial spectra are shown.

The bilayer lipid membrane inserting ability and channel-forming potential of artificial molecular hourglass **2** were primarily evaluated by a vesicle fluorescent assay.[9,11] For this assay, a halogen-sensitive fluorescent dye, lucigenin, was utilized as an indicator, which was encapsulated into vesicles prepared with egg yolk phosphatidylcholine (EYPC). The EYPC vesicles containing $NaNO_3$ buffer solution (pH = 7.0) inside were suspended into M^+Cl^- buffer solution (M = Li, Na, K, Rb, or Cs, pH = 7.0) to establish a M^+Cl^- concentration gradient across the lipid membrane (Fig. S3, ESI†). The M^+Cl^- flow across the vesicle membrane mediated by molecular hourglass **2** was checked by monitoring the fluorescence intensity variation of lucigenin. With the addition of molecular hourglass **2**, the fluorescence intensity decreased gradually with time (Fig. S4, ESI†), which indicated that **2** possessed the ability to embed into the lipid membrane to transport ions across the membrane. However, when the concentration of **2** increased to about 25 μM (ratio of **2** to lipid = 18.5 mol%) in the vesicle fluorescent assay, a precipitation phenomenon was observed, which was possibly caused by the poor solubility of **2** in buffer solutions. Due to this unexpected situation, the attempt to obtain the half-maximal effective concentration (EC_{50}) from fitting of the dose–response curve with the Hill equation failed.

The incorporating capability of artificial molecular hourglass **2** into planar lipid membrane was further investigated through a planar bilayer lipid membrane conductance measurement experiment (BLM). In the BLM tests, 1,2-diphytanoyl-*sn*-*glycero*-3-phosphocholine (DPhPC) was applied to form a planar lipid membrane around a small pore (diameter: *ca.* 200 μm) on a recording cup.[12] The lipid membrane separated the chamber and cup into *cis* and *trans* sides, which were filled with KCl bath solution (1.0 M, 1.0 mL) with an Ag/AgCl electrode immersed into each side. After adding channel molecules into the *cis* chamber side and applying voltage across the planar membrane, channel current signals can be recorded with time. With the addition of molecular hourglass **2** (1.0 μL THF solution, final concentration: 1.0 μM) to the *cis* side and stirring for a few minutes, a voltage in the range of −150 mV to +150 mV was applied successively. In current traces, representative and reproducible square-top channel current signals were observed (Fig. 3a, b and Fig. S6, ESI†), which corresponded to the conversion of the "open" and "closed" state of the ion channel, and definitely confirmed that artificial molecular hourglass **2** spanned the lipid bilayer and transported ions through the channel mechanism. The current–voltage plot is shown in Fig. 3c, which presents a linear current–voltage relationship, giving a slope conductance value of 18.9 ± 0.7 pS by linear fit.

The ion selectivity of artificial molecular hourglass **2** was also studied with a BLM test in asymmetric KCl bath solutions (*cis*/*trans* = 1.0 M/0.25 M). The reversal potential (V_r) was obtained to be −9.37 mV from linear fit of the current–voltage relationship under KCl concentration gradient conditions (Fig. 3d). Using this reversal potential, the Cl^-/K^+ permeability ratio P_{Cl^-}/P_{K^+} was determined to be 0.54 with the Goldman–Hodgkin–Katz equation. This value was relatively smaller than previously reported ones for anion-selective molecular

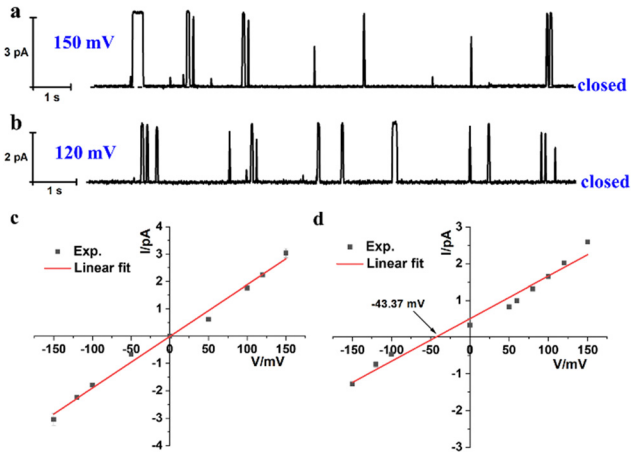

Fig. 3 Current traces of **2** at (a) 150 mV and (b) 120 mV in symmetrical KCl bath solutions (*cis*/*trans* = 1.0 M/1.0 M). *I*–*V* plots under (c) symmetrical (*cis*/*trans* = 1.0 M/1.0 M) and (d) asymmetric (*cis*/*trans* = 1.0 M/0.25 M) KCl bath solutions. Reversal potential V_r = −9.37 mV.[9a,13] The final concentration of **2** is 1.0 μM.

hourglass channels (P_{Cl^-}/P_{K^+} = 1.90[9a] and 4.17[9b], respectively). The permeability ratio unambiguously indicated that opposite to its analogues, artificial molecular hourglass **2** was a cation-selective channel and slightly preferred K^+ transport over Cl^-. The comparatively weak K^+ ion selectivity[14] may be attributed to the following aspects: (1) the electron-rich arms of **2** could not efficiently compensate the dehydration sacrifice of Cl^- as the electron-deficient arms of **1** did, which largely obstructs the transmembrane transport of Cl^-, but facilitates that of K^+ (hydration energy of Cl^- and K^+: 381 *vs.* 322 kJ mol^{-1}); (2) K^+ is smaller than Cl^- in size (radius: 1.38 *vs.* 1.81 Å),[15] so it could pass through the narrow central skeleton more easily. To further verify our presumptions, we investigated the ion selectivity using ion pairs in terms of different hydration ion radii and hydration energies.[15,16] The results showed Cl^-/Mg^{2+} ($P_{Cl^-}/P_{Mg^{2+}}$ = 0.62), K^+/Cs^+ (P_{K^+}/P_{Cs^+} = 1.29), Cl^-/Br^- (P_{Cl^-}/P_{Br^-} = 136.59) and $K^+ > Mg^{2+}$ selectivity. These results highlight the effects of both ion size and hydration energy (Fig. S8, ESI†). Thus, the smaller size and lower hydration energy of K^+, combined with the effective compensation of dehydration sacrifice by the channel molecule may contribute to the weak cation selectivity of **2**.

In conclusion, utilizing a side arm modification strategy to tether relatively flexible and electron-rich phenyl alkyl ether chain side arms to a tetraoxacalix[2]arene[2]triazine macrocyclic model scaffold, a neoteric artificial molecular hourglass was designed and synthesized. This molecular hourglass can effectively embed into an artificial lipid bilayer membrane and participate in transmembrane ion transport through a unimolecular channel mechanism. Possibly due to a balance effect involving ion size, hydration energy, and the efficient compensation of ion dehydration sacrifice, a weak cation selectivity was resulted in contrast to its previously reported analogues with electron-deficient arms. These observations revealed that, by restructuring the side arms of an artificial molecular hourglass, the ion transport selectivity can be conveniently and

purposefully regulated. Thus, these artificial molecular hourglass channels may find applications in modulating ion homeostasis. Moreover, the transport activity of the elegantly designed molecular hourglass in living cells is highly attractive, which is an ongoing interest in our laboratory.

This work was supported by the National Natural Science Foundation of China (22171271, 22022112), Beijing National Laboratory for Molecular Sciences (BNLMSCXXM-202002), and BMS junior fellow scholarship.

Conflicts of interest

There are no conflicts to declare.

Notes and references

1 B. Hille, *Ionic Channels of Excitable Membranes*, Sinauer Associates Inc., Sunderland, MA, 3rd edn, 2001.
2 T. J. Jentsch and M. Pusch, *Physiol. Rev.*, 2018, **98**, 1493–1590.
3 M. Shteinberg, I. J. Haq, D. Polineni and J. C. Davies, *Lancet*, 2021, **397**, 2195–2211.
4 (*a*) T. J. Jentsch, *J. Physiol.*, 2015, **593**, 4091–4109; (*b*) M. Maduke, C. Miller and J. A. Mindell, *Annu. Rev. Biophys. Biomol. Struct.*, 2000, **29**, 411–438.
5 R. Dutzler, E. B. Campbell, M. Cadene, B. T. Chait and R. MacKinnon, *Nature*, 2002, **415**, 287–294.
6 G. Picci, S. Marchesan and C. Caltagirone, *Biomedicines*, 2022, **10**, 885.
7 H. Zhang, X. Li, J. Hou, L. Jiang and H. Wang, *Chem. Soc. Rev.*, 2022, **51**, 2224–2254.
8 (*a*) P. H. Schlesinger, R. Ferdani, J. Liu, J. Pajewska, R. Pajewski, M. Saito, H. Shabany and G. W. Gokel, *J. Am. Chem. Soc.*, 2002, **124**, 1848–1849; (*b*) N. Sakai, D. Houdebert and S. Matile, *Chem. – Eur. J.*, 2003, **9**, 223–232; (*c*) N. Sakai, N. Sorde, G. Das, P. Perrottet, D. Gerard and S. Matile, *Org. Biomol. Chem.*, 2003, **1**, 1226–1231; (*d*) J. A. Malla, R. M. Umesh, A. Vijay, A. Mukherjee, M. Lahiri and P. Talukdar, *Chem. Sci.*, 2020, **11**, 2420–2428; (*e*) A. Roy, H. Joshi, R. Ye, J. Shen, F. Chen, A. Aksimentiev and H. Zeng, *Angew. Chem., Int. Ed.*, 2020, **59**, 4806–4813; (*f*) C. Zhang, J. Tian, S. Qi, B. Yang and Z. Dong, *Nano Lett.*, 2020, **20**, 3627–3632.
9 (*a*) W.-L. Huang, X.-D. Wang, Y.-F. Ao, Q.-Q. Wang and D.-X. Wang, *J. Am. Chem. Soc.*, 2020, **142**, 13273–13277; (*b*) W.-L. Huang, X.-D. Wang, Y.-F. Ao, Q.-Q. Wang and D.-X. Wang, *Angew. Chem., Int. Ed.*, 2023, **62**, e202302198.
10 (*a*) R.-B. Xu, Q.-Q. Wang, Y.-F. Ao, Z.-Y. Li, Z.-T. Huang and D.-X. Wang, *Org. Lett.*, 2017, **19**, 738–741; (*b*) D.-H. Tuo, W. Liu, X.-Y. Wang, X.-D. Wang, Y.-F. Ao, Q.-Q. Wang, Z.-Y. Li and D.-X. Wang, *J. Am. Chem. Soc.*, 2019, **141**, 1118–1125.
11 (*a*) X.-D. Wang, S. Li, Y.-F. Ao, Q.-Q. Wang, Z.-T. Huang and D.-X. Wang, *Org. Biomol. Chem.*, 2016, **14**, 330–334; (*b*) W.-L. Huang, X.-D. Wang, S. Li, R. Zhang, Y.-F. Ao, J. Tang, Q.-Q. Wang and D.-X. Wang, *J. Org. Chem.*, 2019, **84**, 8859–8869.
12 J. K. W. Chui and T. M. Fyles, *Chem. Soc. Rev.*, 2012, **41** 148–175.
13 The observed reversal potential −43.37 mV after correction by differential chloride potential −34 mV.
14 (*a*) Y. Tanaka, Y. Kobuke and M. Sokabe, *Angew. Chem., Int. Ed. Engl.*, 1995, **34**, 693–694; (*b*) N. Yoshino, A. Satake and Y. Kobuke, *Angew. Chem., Int. Ed.*, 2001, **40**, 457–459; (*c*) P. Xin, Y. Sun, H. Kong, Y. Wang, S. Tan, J. Guo, T. Jiang, W. Dong and C.-P. Chen, *Chem. Commun.*, 2017, **53**, 11492–11495.
15 Y. Marcus, *Chem. Rev.*, 1988, **88**, 1475–1498.
16 D. W. Smith, *J. Chem. Educ.*, 1977, **54**, 540–542.

